The Astrophysical Journal, 627:834–844, 2005 July 10

HIGH SPATIAL RESOLUTION OBSERVATIONS OF NH_3 AND CH_3OH TOWARD THE MASSIVE TWIN CORES NGC 6334I AND NGC 6334I(N)

H. Beuther, S. Thorwirth, Q. Zhang, T. R. Hunter, and S. T. Megeath
Harvard-Smithsonian Center for Astrophysics, 60 Garden Street, Cambridge, MA 02138; hbeuther@cfa.harvard.edu

A. J. Walsh
School of Physics, University of New South Wales, Kensington, NSW 2052, Australia

and

K. M. Menten
Max-Planck-Institut für Radioastronomie, Auf dem Hügel 69, 53121 Bonn, Germany
Received 2005 February 18; accepted 2005 April 4

ABSTRACT

Molecular line observations of NH_3 $(J, K) = (1, 1)$ and (2, 2) and CH_3OH at 24.93 GHz taken with the Australian Telescope Compact Array (ATCA) toward the massive twin cores NGC 6334I and NGC 6334I(N) reveal significant variations in the line emission between the two massive cores. The UC H II region/hot core NGC 6334I exhibits strong thermal NH_3 and CH_3OH emission adjacent to the UC H II region and coincident with two millimeter continuum peaks observed by T. R. Hunter et al. In contrast, we find neither compact NH_3 nor thermal CH_3OH line emission toward NGC 6334I(N). There the NH_3 emission is distributed over a broad region (>1′) without a clear peak, and we find Class I CH_3OH maser emission with peak brightness temperatures up to 7000 K. The maser emission peaks appear to be spatially associated with the interfaces between the molecular outflows and the ambient dense gas. Peak NH_3 (1, 1) line brightness temperatures $\geq$70 K in both regions indicate gas temperatures on the same order. NH_3 emission is also detected toward the outflow in NGC 6334I, resulting in an estimated rotational temperature of $T_{\rm rot} \sim 19$ K. Furthermore, we observe CH_3OH and NH_3 absorption toward the UC H II region; the velocity structure is consistent with expanding molecular gas around the UC H II region. Thermal and kinematic effects possibly imposed from the UC H II region on the molecular core are also discussed.

Subject headings: ISM: individual (NGC 6334I, NGC 6334I(N)) — line: profiles — masers — stars: early-type — stars: formation — techniques: interferometric

1. INTRODUCTION

The prominent molecular cloud/H II region complex NGC 6334 at a distance of 1.7 kpc is composed of a series of luminous star-forming regions at various stages of evolution (Neckel 1978; Straw & Hyland 1989). During the initial radio and infrared studies completed over 20 years ago, a confusing family of nomenclature was introduced for this region. The letters A–F refer to Very Large Array (VLA) 6 cm continuum sources (Rodríguez et al. 1982), while roman numerals I–VI refer to far-infrared sources (McBreen et al. 1979; Loughran et al. 1986). While each center of activity contains CO hot spots and various masers, the youngest region appears to be radio source F (which corresponds to infrared source I and IRAS source 17175−3544), located at the northeastern end of the complex. Even the earliest far-infrared maps (Gezari 1982) resolved the emission of source I into two cores: the sources I and I(N), which are separated by ∼90″. With the cold dust emission, only a few red infrared sources, and weak centimeter-continuum emission (e.g., Gezari 1982; Tapia et al. 1996; Sandell 2000; Carral et al. 2002), source I(N) is considered the least evolved object in the region.

1.1. *NGC 6334I*

A well-known cometary compact H II region lies at the heart of source I (e.g., Carral et al. 1997) and contains associated OH masers (Brooks & Whiteoak 2001; Gaume & Mutel 1987), Class II CH_3OH masers (Ellingsen et al. 1996), and H_2O masers (Moran & Rodríguez 1980; Forster & Caswell 1989). Recent mid-infrared imaging with OSCIR at the Keck II telescope has identified a candidate star (IRS 1E) for the excitation source of the compact H II region (De Buizer et al. 2002). Single-dish bolometer maps from the James Clerk Maxwell Telescope (JCMT) reveal a compact (<20″) strong (sub)millimeter continuum source with an estimated dust temperature of 100 K (Sandell 2000). A Swedish-ESO Submillimeter Telescope (SEST) line survey (Thorwirth et al. 2003) shows rich molecular line emission in the millimeter wavelength range similar to prototypical high-mass star-forming regions such as Orion KL. Comparable results are obtained in a miniline survey near 345 GHz (McCutcheon et al. 2000). A CO (2–1) outflow with a velocity range of ∼150 km s^{-1} emanates from NGC 6334I (Bachiller & Cernicharo 1990), and a similar outflow is also seen in the H76α and H92α recombination lines (de Pree et al. 1995). Several knots of shock-excited H_2 emission have been detected near the ends of this outflow (Davis & Eisloeffel 1995; Persi et al. 1996; Megeath & Tieftrunk 1999), along with NH_3 (3, 3) masers (Kraemer & Jackson 1995). The driving source(s) for the outflow were claimed to be either the powering source of the UC H II region or that of an adjacent object. One candidate is the cold 20 μm source I:KDJ2 located 6.″5 to the northwest of the UC H II region (as resolved by the Mid-Infrared Array Camera [MIRAC2] at the Infrared Telescope Facility), which is not seen at shorter wavelengths (Kraemer et al. 1999). Alternatively, the powering source of the UC H II region and I:KDJ2 may both drive independent outflows.

1.2. *NGC 6334I(N)*

Similar to source I, the JCMT bolometer maps show I(N) to be a strong source of (sub)millimeter-continuum emission

(Sandell 2000). The estimated dust temperature is lower around 30 K. While source I is stronger than I(N) in CS (5–4) (Kraemer & Jackson 1999) and in CS (7–6), the HC_3N (15–14) line is much stronger in I(N) than in I (Megeath & Tieftrunk 1999; Sollins & Megeath 2004). Further differences can be seen in the 230 GHz line survey, in which the CH_3OH bands (at 240–242 and 250–252 GHz) are fainter in I(N) than I (Thorwirth et al. 2003), probably indicating a younger age for this region. Similar conclusions were drawn by McCutcheon et al. (2000) on the basis of their smaller line survey and spectral line mapping of the two regions. Indeed, in striking contrast to I, the I(N) region shows no mid-infrared emission and only a few red infrared sources (Tapia et al. 1996). Traditionally, I(N) has also been known to lack centimeter-continuum emission; however, two faint ($\sim$0.3 mJy) compact centimeter sources have recently been detected with the VLA (Carral et al. 2002). One object lies only 7″ from the (sub)millimeter-continuum peak and is consistent with the ionizing radiation from a B2 zero-age main-sequence star. This centimeter peak is associated with Class II CH_3OH maser emission (Ellingsen et al. 1996). Furthermore, Class I CH_3OH maser emission has been mapped at 44 GHz and shows emission peaks distributed over approximately 30″ (Kogan & Slysh 1998). A bipolar outflow has also been mapped in the SiO (2–1) and (5–4) transitions with SEST in the southeast-northwest direction, approximately coincident with the distribution of the Class I CH_3OH maser at 44 GHz (Megeath & Tieftrunk 1999). These authors also find independent evidence for outflow activity in H_2 clumps, which are present but less pronounced than those in source I.

1.3. *Concerted ATCA and SMA Observations*

Because NGC 6334I and NGC 6334I(N) are close to each other, thus sharing a similar large-scale environment, but are in different evolutionary stages, they are the ideal target sources to characterize the evolutionary differences in physical and chemical properties of massive star-forming regions. Both sources have been thoroughly investigated at near- to mid-infrared wavelengths and at lower spatial resolution in the radio and millimeter regime (with some already mentioned exceptions). However, high spatial resolution molecular line and continuum studies from short centimeter to submillimeterwavelengths have been lacking so far because of its location in the southern hemisphere. This situation has changed over the last couple of years with the advent of the 12 and 3 mm systems at the Australian Telescope Compact Array (ATCA) and the dedication of the Submillimeter Array (SMA). Therefore, we started a combined effort to investigate the molecular line and continuum emission from 12 mm to the submillimeter regime employing both instruments. Here we present the NH_3 (1, 1) and (2, 2) and the CH_3OH (near 25 GHz) results from ATCA, whereas a separate paper outlines the first SMA results toward these sources at 217 GHz (T. R. Hunter et al. 2005, in preparation).

The SMA data show three millimeter-continuum sources toward NGC 6334I, two of them adjacent to the UC H II region and one approximately coincident with the centimeter-continuum peak (T. R. Hunter et al. 2005, in preparation). Toward NGC 6334I(N), they detect another millimeter-continuum peak (offset by a few arcseconds from the centimeter peak) with a little bit of more extended emission. These millimeter-peak positions are compared with our NH_3 and CH_3OH emission throughout this paper. Furthermore, T. R. Hunter et al. (2005, in preparation) detect very collimated SiO (5–4) outflows in NGC 6334I and NGC 6334I(N), and the outflow orientation in both sources is approximately the same, in the northeast-southwest direction. It is important to mention that the new outflow in NGC 6334I(N) is approximately perpendicular to the previously observed larger scale outflow (Megeath & Tieftrunk 1999).

TABLE 1
Phase Reference Centers

Source	R.A. (J2000.0)	Decl. (J2000.0)
NGC 6334I	17 20 53.44	−35 47 02.2
NGC 6334I(N)	17 20 54.63	−35 45 08.9

Note.—Units of right ascension are hours, minutes, and seconds, and units of declination are degrees, arcminutes, and arcseconds.

2. OBSERVATIONS

The sources NGC 6334I and NGC 6334I(N) were observed on 2004 July 6 and 7 with ATCA in the compact 750D configuration with five antennas and a baseline range between 31 and 719 m. Antenna 6 was also included, resulting in a maximum projected baseline of $\sim$4.3 km. The phase reference centers are given in Table 1. The observed lines are the NH_3 (1, 1) and (2, 2) inversion lines, with the frequencies of the main hyperfine components at 23.695 and 23.723 GHz and one spectral setup at 24.932 GHz, covering three CH_3OH lines at 24.9287 GHz [CH_3OH ($3_{2,1}$–$3_{1,2}$) E], 24.9335 GHz [CH_3OH ($4_{2,2}$–$4_{1,3}$) E], and 24.9344 GHz [CH_3OH ($2_{2,0}$–$2_{1,1}$) E]. In addition, we observed the centimeter-continuum emission with one spectral unit, covering a bandwidth of 128 MHz centered at 22.08 GHz. A good u-v coverage was obtained through regular switching between both sources and the three spectral setups. The spectral resolution of the observations was 16 kHz, corresponding to a velocity resolution of $\sim$0.2 km s^{-1}. The primary beam of ATCA at the given frequency is $\sim$130″. The data were reduced with the MIRIAD package. When we apply a robust weighting of 1 (closer to natural than uniform weighting, thus stressing the shorter baselines), the synthesized beam is 2.″8 × 2.″2. We smoothed the data to 0.5 km s^{-1} channels, and the rms per 0.5 km s^{-1} is $\sim$6 mJy. The rms of the 22 GHz continuum and some of the velocity-integrated line maps are partly slightly higher, mainly because of more pronounced sidelobe effects due to the strong emission features. The 3 σ values are given separately in each figure.

3. OBSERVATIONAL RESULTS

The spatial distribution of the molecular gas is significantly different for NGC 6334I and NGC 6334I(N) (Figs. 1 and 2). Toward NGC 6334I, we find strong thermal compact NH_3 and CH_3OH emission in close proximity to the UC H II region. In contrast, the NH_3 emission toward NGC 6334I(N) exhibits very extended emission without a compact component, and we find no thermal CH_3OH feature but only strong maser emission.

3.1. *NGC 6334I*

The NH_3 and CH_3OH emission from NGC 6334I shows two emission peaks offset by a few arcseconds from the UC H II region (Fig. 1). The low-level molecular emission terminates at the edge of the UC H II region; thus, we have an example of an observed edge-on orientation between a UC H II region next to a hot core. The two molecular line peaks are coincident with two of the three millimeter-continuum peaks observed by T. R. Hunter et al. (2005, in preparation) with the SMA. Interestingly, the molecular line peaks are of the same intensity, whereas the

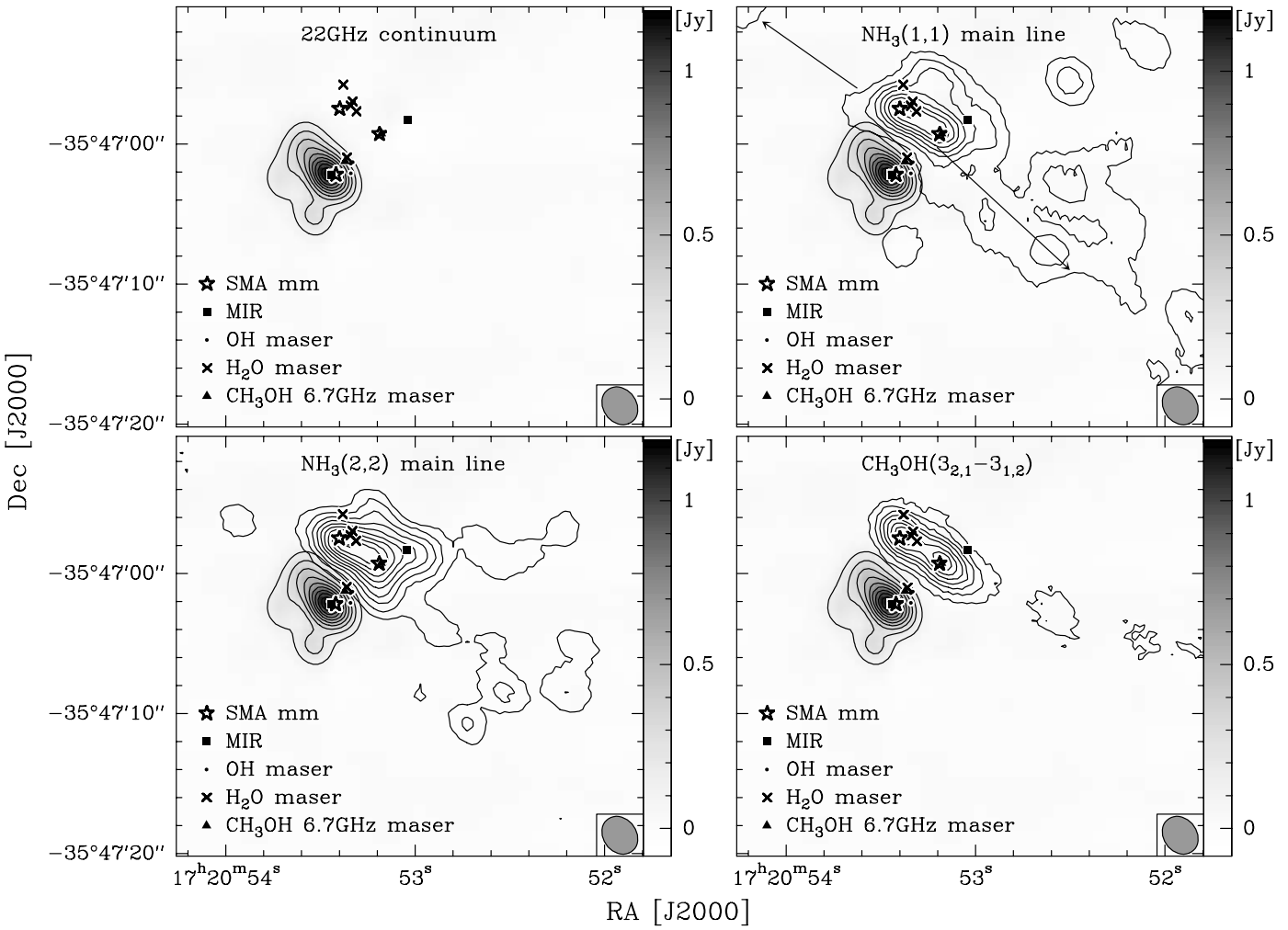

FIG. 1.—Centimeter continuum (gray scale and contours in the top left image, gray scale in the other panels), integrated main hyperfine component NH_3 (1, 1) (*top right*) and (2, 2) (*bottom left*) and CH_3OH ($3_{2,1}$–$3_{1,2}$) *E* integrated line emission toward NGC 6334I. The arrows at top right outline the direction of the red and blue outflow lobes (which are apparently a little bit bent; T. R. Hunter et al. 2005, in preparation). The contour levels are from 10% to 90% (step 10%) from the peak emission of 1197 mJy beam^{-1} for the centimeter-continuum image ($3\sigma \sim 42$ mJy beam^{-1}) and in 3 σ steps for the line emission. The approximate 3 σ values for the NH_3 (1, 1) and (2, 2) and CH_3OH lines are 21, 12, and 10 mJy beam^{-1}, respectively. The symbols and spectral lines are labeled in each panel. The synthesized beams are shown at bottom right of each panel as well.

northeastern millimeter peak has about 2.5 times the continuum flux of the southwestern millimeter peak. Another difference between the two peak positions is that the northeastern peak is associated with H_2O maser emission (Moran & Rodríguez 1980; Forster & Caswell 1989), whereas the southwestern peak exhibits Class II CH_3OH maser emission (Ellingsen et al. 1996). More CH_3OH, H_2O, and OH maser emission is found at the interface between the molecular core and the UC H II region. Furthermore, we detect extended NH_3 (1, 1) emission southwest of the two peak positions. This extended emission is significantly weaker in the NH_3 (2, 2) line and is barely detected in CH_3OH. It is in the same direction as the molecular outflow observed in CO by Bachiller & Cernicharo (1990) and more recently in SiO by T. R. Hunter et al. (2005, in preparation).

The spatial distribution of the NH_3 gas that we have observed varies considerably from the previously reported VLA map by Jackson et al. (1988). With a spatial resolution of $5\farcs2 \times 7\farcs7$, they detected more extended emission, and their peak intensity position is $\sim 5''$ south of ours. Tapering our data to the same lower spatial resolution, we recover most of their extended structure, but our peak positions remain coincident with the two peaks shown in Figure 1. Due to the large number of antennas at the VLA (27 vs. 6 at the ATCA), their *u-v* coverage should be good and allow a reasonable recovery of the large-scale structure, but the offset of their peak position remains a puzzle. However, our data are less sensitive to large-scale emission and therefore trace the small-scale cores far better. In addition, the exact coincidence of our NH_3 and CH_3OH peak positions with the millimeter peaks reported by T. R. Hunter et al. (2005, in preparation) gives additional confidence to the small-scale gas core distribution presented in Figure 1. Furthermore, when we consider the multiple sources that we find in NGC 6334I and the now known outflow in the region (Bachiller & Cernicharo 1990), the disk interpretation of the NH_3 data by Jackson et al. (1988) does not hold anymore, and it is more likely that their observed large-scale emission is somehow associated with the outflow as well.

3.2. *NGC 6334I(N)*

We do not detect any compact thermal NH_3 or CH_3OH emission toward NGC 6334I(N) (Fig. 2). However, the extended NH_3 emission has about the same peak intensities as NGC 6334I but is distributed over a large area (>1′) without a distinct peak position. The millimeter peak detected by T. R. Hunter et al. (2005, in preparation) is located approximately at the center of

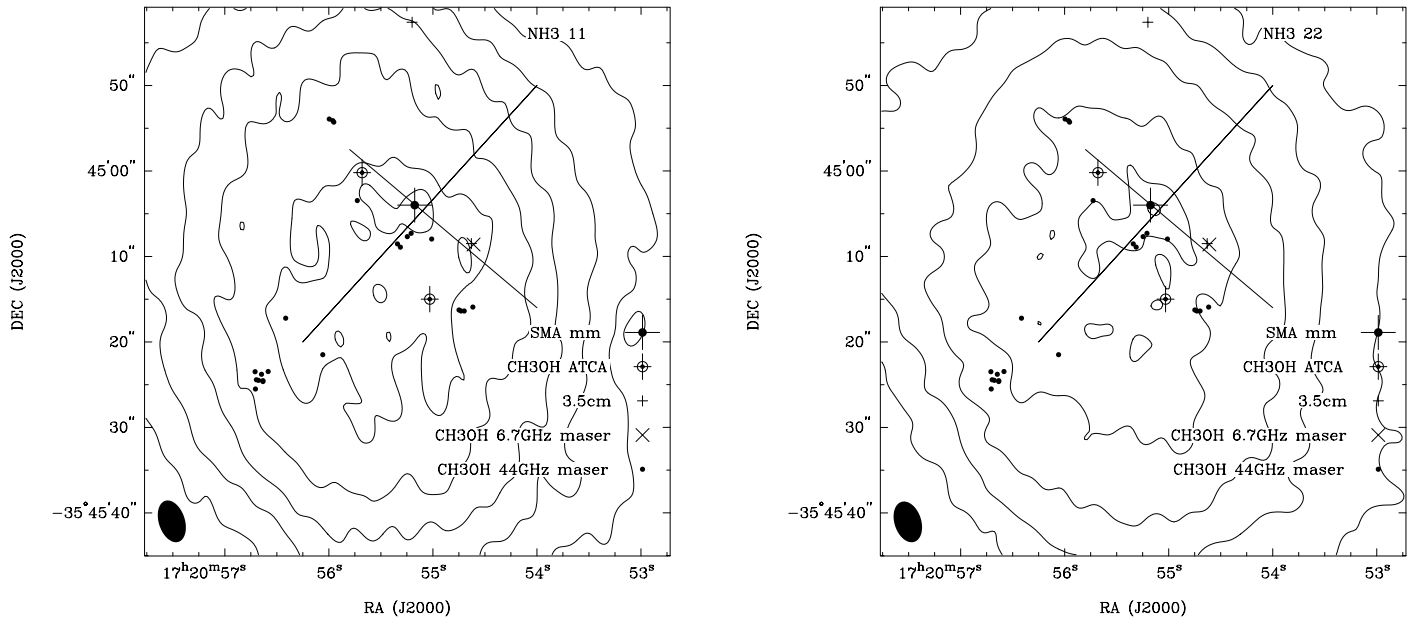

FIG. 2.—Integrated main hyperfine component NH_3 (1, 1) (*left*) and (2, 2) line emission (*right*) toward NGC 6334I(N). The two lines outline the directions of the two observed outflows in the region (northeast-southwest [T. R. Hunter et al. 2005, in preparation] and southeast-northwest [Megeath & Tieftrunk 1999]). The contour levels are 58, 58, and 348 mJy beam^{-1} ($3\sigma \sim 9$ mJy beam^{-1}) and 33, 33, and 198 mJy beam^{-1} ($3\sigma \sim 6$ mJy beam^{-1}) for the NH_3 (1, 1) and (2, 2) components, respectively. The symbols are marked at bottom right of each panel. The synthesized beams are shown at bottom left of each panel as well.

the large-scale NH_3 core. The NH_3 (1, 1) and (2, 2) emission has a spatial distribution similar to that of the NH_3 (3, 3) emission previously reported by Kraemer & Jackson (1999).

While we do not detect any thermal CH_3OH emission, we find Class I CH_3OH maser emission from the CH_3OH ($3_{2,1}$–$3_{1,2}$) *E* and CH_3OH ($4_{2,2}$–$4_{1,3}$) *E* lines [nothing from the CH_3OH ($2_{2,0}$–$2_{1,1}$) *E* line]. Both lines show a maser component at approximately -3 km s^{-1}, but the CH_3OH ($4_{2,2}$–$4_{1,3}$) *E* line exhibits another maser component at approximately -5 km s^{-1} (Fig. 3). The spatial positions of the -3 km s^{-1} components are

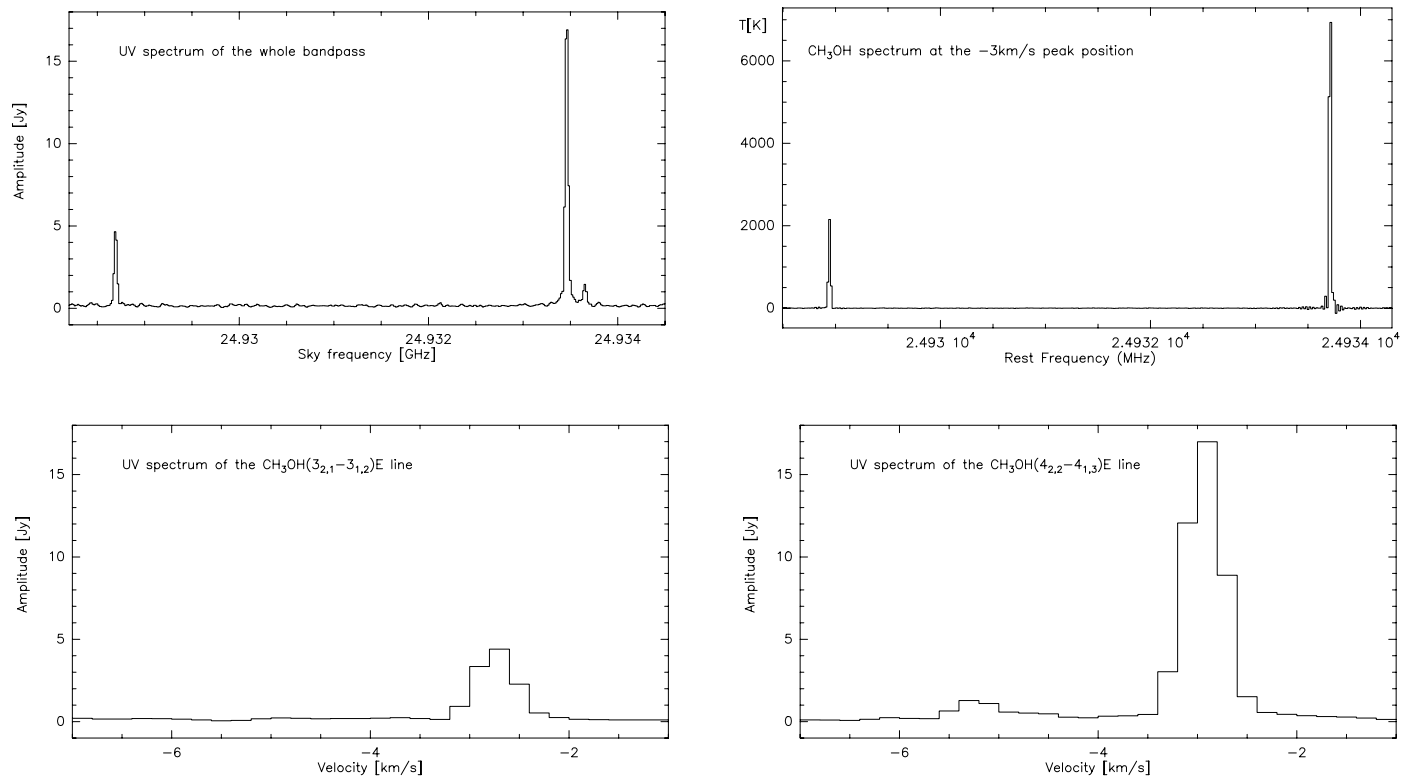

FIG. 3.—CH_3OH maser spectra taken toward the NGC 6334I(N). *Top left*, Spectrum showing the *u-v* spectrum on the shortest baseline of 31 m presenting all detected components; *top right*, spectrum taken after imaging toward the northeastern CH_3OH maser position [the conversion factor for K (Jy beam^{-1})$^{-1}$ for the right spectrum is $\sim$385]. The two bottom spectra are the same *u-v* spectra as the top left one but this time are presented on the velocity scale and differentiated between the CH_3OH ($3_{2,1}$–$3_{1,2}$) *E* (*bottom left*) and CH_3OH ($4_{2,2}$–$4_{1,3}$) *E* lines (*bottom right*).

TABLE 2
CH_3OH Class I Maser Positions

Velocity (km s^{-1})	R.A. (J2000.0)	Decl. (J2000.0)
−3	17 20 55.68	−35 45 00.2
−5	17 20 55.03	−35 45 15.0

Note.—Units of right ascension are hours, minutes, and seconds, and units of declination are degrees, arcminutes, and arcseconds. The estimated absolute positional accuracy is ∼0.″2.

approximately 7″ northeast of the millimeter peak in the direction of the collimated SiO outflow, whereas the −5 km s^{-1} component is located about 10″ south of the millimeter peak (the exact positions are given in Table 2). The observed peak brightness temperature of the −3 km s^{-1} line is ∼7000 K (Fig. 3). The −5 km s^{-1} component is less clearly associated with one of the two outflow axes, but both components are spatially close to previously detected Class I CH_3OH (7_0–6_1) A^+ 44 GHz maser positions (Kogan & Slysh 1998). We note that there are significantly fewer, just two, 25 GHz maser components detected than 44 GHz components. The 23 maser spots observed in the latter line are spread over an area of 23″×32″, which is somewhat larger but comparable to the ∼15″ separation of the 25 GHz components. The positional offsets between the 44 and 25 GHz maser positions may be due to the loss of absolute positional information during self-calibration of the 44 GHz data by Kogan & Slysh (1998). Performing Gaussian fits to the CH_3OH data in the image plane, we get slightly extended features compared to the beam size. This indicates unresolved spatial blending of different maser components within each channel width of 0.2 km s^{-1}.

4. ANALYSIS

4.1. *Temperature Estimates from the* NH_3 *Observations*

4.1.1. *The NGC 6334I Peak Region*

The NH_3 (1, 1) and (2, 2) lines are widely used as thermometers in molecular clouds (e.g., Walmsley & Ungerechts 1983; Danby et al. 1988). Figure 4 shows NH_3 (1, 1) and (2, 2) spectra toward the two NH_3 peak positions overlaid with fits to the hyperfine structure. The hyperfine structure line fits were performed in CLASS (part of the GILDAS software package) assuming a Gaussian velocity distribution, equal excitation temperatures, and the theoretical intensity ratio and spacing between main and satellite hyperfine lines. The fitted parameters are the excitation temperature, the opacity of the main hyperfine component, the line width, and the $v_{\rm LSR}$. Obviously, the flat-topped fits do not reproduce the observed spectra well, which is likely due to an extremely high optical depth and varying excitation conditions over the width of the lines. Missing flux due to missing short spacings does not play a significant role since we sample large-scale emission in NGC 6334I(N) (Fig. 2) and the *u-v* coverage of each observation is nearly the same. These fits do not allow us to derive accurate temperatures. Therefore, we tried to work only with the satellite hyperfine components of the spectra, and Figure 5 presents the integrated emission maps of the outer satellite hyperfine components at the most negative velocities [the blend of the NH_3 (1, 1) $F, F_1 = 0.5, 0$–$0.5, 1$ and $F, F_1 = 0.5, 0$–$1.5, 1$ lines at ∼23.696 GHz and the NH_3 (2, 2) $F = 2$–1 line at ∼23.725 GHz]. In the following, we refer to these lines as the (outermost) satellite hyperfine (hf) components. An intriguing difference between the integrated NH_3 (1, 1) and (2, 2) satellite hyperfine structure line maps is that the (1, 1) satellite hf line shows a similar peak intensity distribution as the (1, 1) main hf

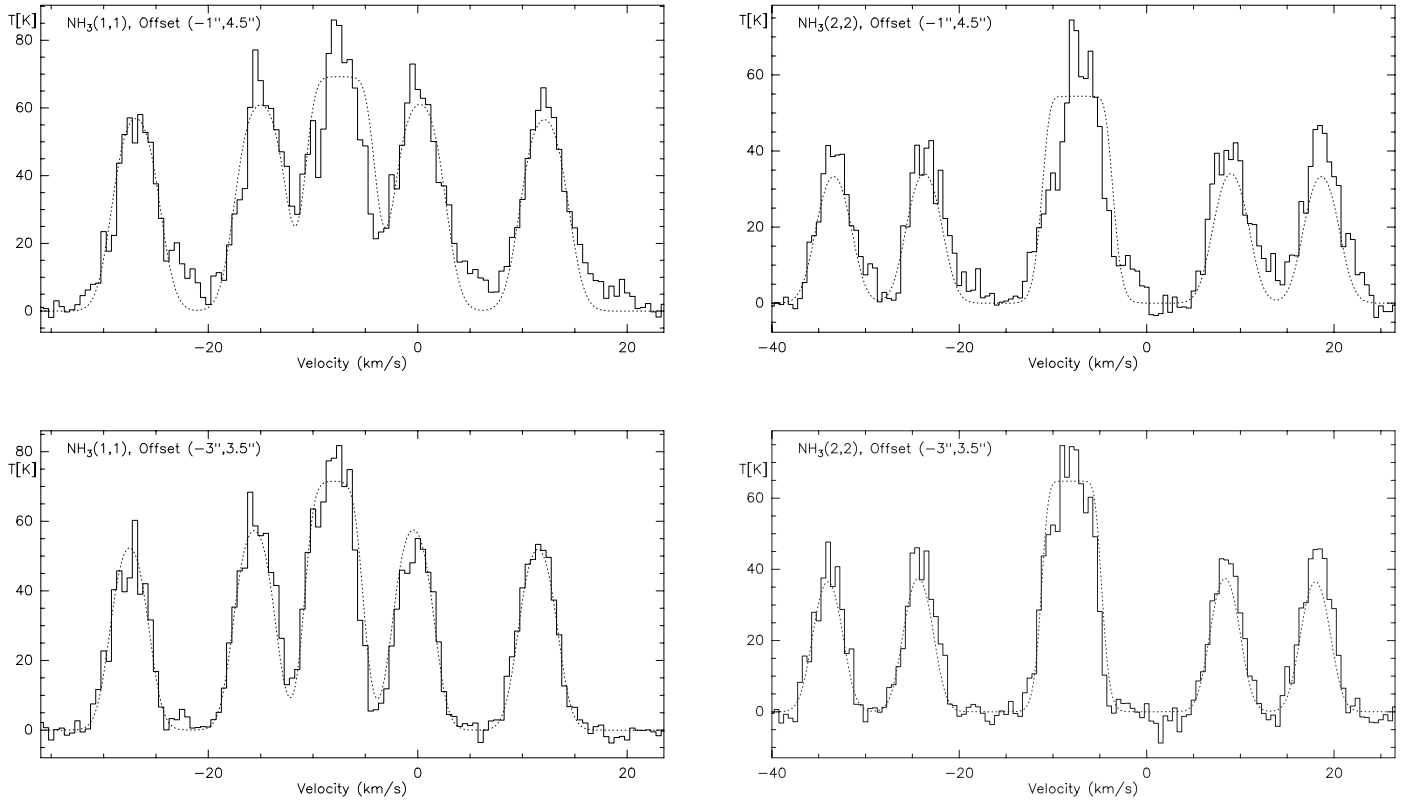

Fig. 4.—NH_3 spectra toward the two peak positions in NGC 6334I (the offsets of the phase reference centers listed in Table 1 are marked in each panel). The rather poor fits are shown as dotted lines.

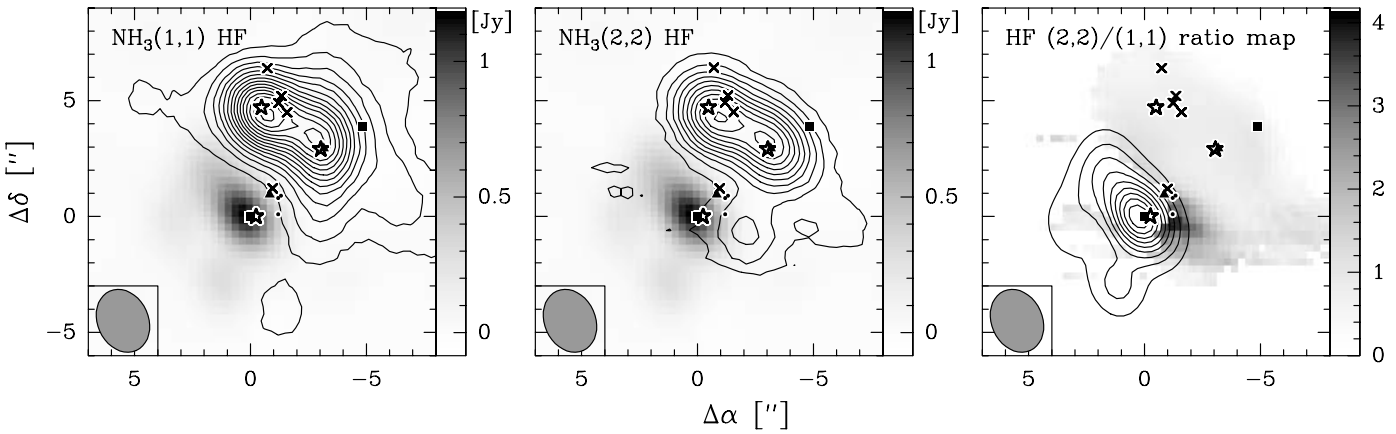

FIG. 5.—Integrated images of the outer satellite hyperfine components at the most negative velocities toward NGC 6334I, showing satellite hyperfine components of NH_3 (1, 1) [the blend of the NH_3 (1, 1) $F, F_1 = 0.5, 0$–0.5, 1 and $F, F_1 = 0.5, 0$–1.5, 1 lines at ~23.696 GHz; *left*] and (2, 2) [the NH_3 (2, 2) $F = 2$–1 line at ~23.725 GHz); *middle*]. The contour levels for the NH_3 (1, 1) and (2, 2) satellite components are in 3 σ steps with $3\sigma(1,1) \sim 10$ and $3\sigma(2,2) \sim 9$ mJy beam^{-1}. *Right*, Ratio map of the two integrated satellite hyperfine images (2, 2)/(1, 1). The centimeter-continuum emission is presented in gray scale in the left and middle panels and in contours (10%–90% from the peak emission of 1197 mJy beam^{-1}) in the right panel. The symbols are the same as in Fig. 1.

line, whereas the (2, 2) satellite hf line shows an additional intensity peak a few arcseconds south, directly at the western edge of the UC H II region peak. A (2, 2)/(1, 1) hf ratio map between the two integrated hf maps stresses this difference as well (Fig. 5, *right*). The peak NH_3 (2, 2)/(1, 1) hf ratios at this position are ~4, in contrast to ratios of ~0.8 toward the two main peak positions.

The energy levels of the NH_3 (1, 1) and (2, 2) lines are 23 and 64 K above ground, and this line pair is mainly sensitive to temperatures below 50 K. As shown by Danby et al. (1988), rotational temperatures derived from NH_3 (1, 1) and (2, 2) line observations are not sensitive to kinetic temperature changes above about 50 K. Therefore, NH_3 (2, 2)/(1, 1) hf ratios >0.4 are of no use for temperature estimates. This is the case for both millimeter-peak positions, as well as the additional (2, 2) hf line peak close to the UC H II region (Fig. 5). However, we observe NH_3 (1, 1) peak brightness temperatures >70 K toward the two millimeter-peak positions, and these brightness temperatures can be considered lower limits for the kinetic temperatures at these positions. As the (2, 2)/(1, 1) hf ratio toward the additional (2, 2) hf line peak is significantly higher (~4), the temperatures there should be higher as well. While it is likely that massive protostellar objects at the center of the two millimeter peaks cause the high temperatures there, the hot spot close to the UC H II region is probably caused by heating of the UC H II region itself.

The energy levels above ground for the three CH_3OH lines are between 28 and 44 K; thus, these lines cannot be used for more accurate temperature determinations as well.

4.1.2. *The NGC 6334I Outflow Region*

The situation is different in the outflow region, and we can extract reasonable NH_3 (1, 1) and (2, 2) spectra toward the NH_3 (1, 1) outflow–associated peak at offsets (−10″, −6″). Fitting the whole hyperfine spectra at this position, we can derive a rotational temperature of $T_{rot} \sim 19$ K (for details on the temperature calculation from NH_3 observations, see, e.g., Ungerechts et al. [1986]). At these low temperatures, rotational temperatures correspond well to kinetic temperatures (Danby et al. 1988).

4.1.3. *The Northern Source NGC 6334I(N)*

Since we have no well-defined NH_3 peak position in NGC 6334I(N), we extracted spectra toward the millimeter-peak position determined by T. R. Hunter et al. (2005, in preparation), which is offset by (6.″5, 5″) from our phase reference center. The brightness temperatures are comparable to the brightness temperatures in the southern source, NGC 6334I, but the opacities are lower, as observed in the lower hyperfine line strengths [especially in the (2, 2) lines; Fig. 6]. Therefore, we can fit these lines reasonably well and again derive rotational temperatures,

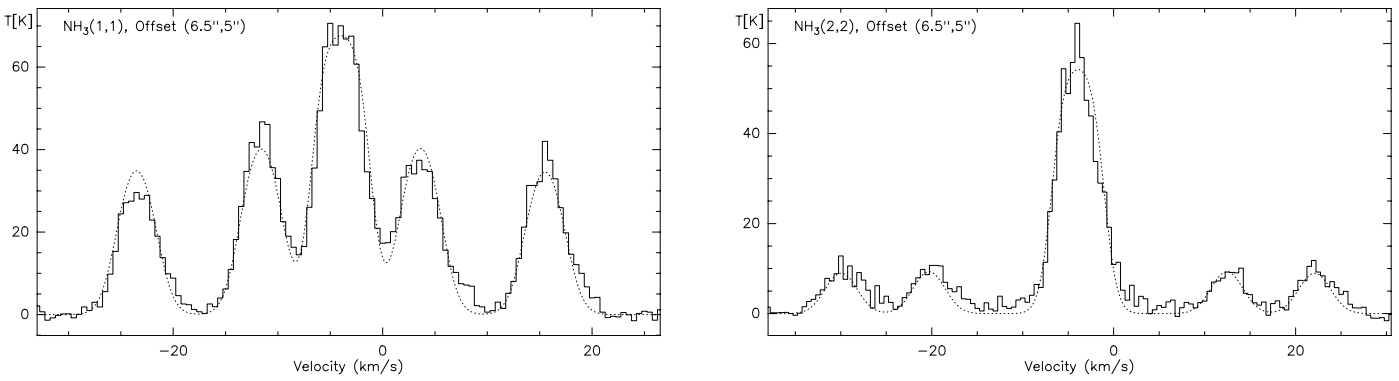

FIG. 6.—NH_3 (1, 1) and (2, 2) spectra taken toward the nominal position of the millimeter-continuum peak discovered by T. R. Hunter et al. (2005, in preparation) toward NGC 6334I(N). The offsets of the phase reference centers listed in Table 1 are marked in each panel. The fits are shown as dotted lines.

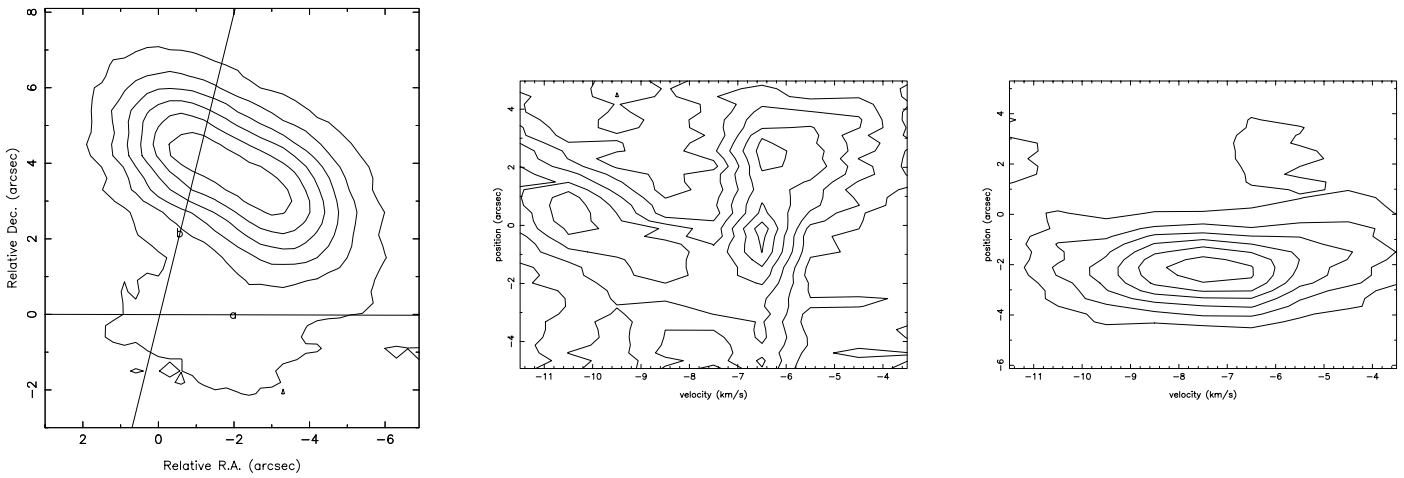

FIG. 7.—*Left*, Plot of *p-v* cuts through the NH_3 (2, 2) outer satellite hyperfine line data cube [NH_3 (2, 2) $F = 2$–1, integrated from −12 to −5 km s^{-1}] of NGC 6334I along the axes outlined; *middle*, cut in the east-west direction; *right*, cut in the northwest-southeast direction. The contour levels are in 11.5, 5.0, and 16.5 mJy $beam^{-1}$ steps for the left, middle, and right panels, respectively.

as previously done for the outflow position. The derived NH_3 rotational temperature is $T_{rot} \sim 47$ K, corresponding to kinetic temperatures $T_{kin} > 100$ K (Danby et al. 1988). Thus, we can again derive only lower limits for the temperatures toward NGC 6334I(N). This estimate, based on the high spatial resolution interferometric observations, is significantly higher than previous estimates of 30 K from single-dish NH_3 observations with a beam size of 55″ (Kuiper et al. 1995), because the latter observations are averaged over the whole region.

4.2. *Kinematic Structures of the Molecular Gas in NGC 6334I*

The striking edge-on orientation between the UC H II region and the molecular peaks in NGC 6334I allows a closer analysis of possible kinematic signatures that the UC H II region might impose on the molecular cores (in addition to the heating effect that we have described in § 4.1.1). Figure 7 shows two position-velocity (*p-v*) cuts performed for NH_3 (2, 2): that in the east-west direction from the UC H II region through the NH_3 (2, 2) hyperfine emission hot spot (*middle*) and that from the UC H II region in the northwestern direction through the main millimeter- and NH_3 peak position (*right*). While there is considerable structure in the east-west *p-v* diagram (Fig. 7, *middle*), it, however, does not reveal any clear signature that the UC H II region could have imposed on the molecular gas. The other *p-v* diagram (Fig. 7, *right*) shows no strong velocity gradients from the UC H II region in the direction of the NH_3 peak position as well.

Figure 8 presents the second-moment maps (velocity dispersion maps) of the two NH_3 (1, 1) and (2, 2) outermost satellite hyperfine lines and one of the CH_3OH lines. While the velocity dispersion of the (1, 1) hf line peaks toward the northeastern NH_3 peak, the (2, 2) velocity dispersion peaks farther south, toward the UC H II region and the NH_3 (2, 2) hyperfine hot spot. In contrast, the second-moment map of CH_3OH shows two peaks, both associated with the two molecular peak positions.

At estimated temperatures of ∼100 K the critical densities of the CH_3OH lines are on the order of 10^4 cm^{-3}, whereas the critical densities of the NH_3 lines are lower (on the order of 10^3 cm^{-3}). The velocity dispersion of the higher density tracer CH_3OH is dominated by internal motion due to the embedded protostars. To some degree this is also the case for NH_3, and especially the (1, 1) second-moment maps peaks toward the strongest millimeter-continuum peak. However, there is no obvious (1, 1) velocity dispersion peak toward the secondary millimeter-peak position. The NH_3 (2, 2) velocity dispersion is clearly dominated by the NH_3 (2, 2) hyperfine hot spot close to the UC H II region. Since NH_3 has lower critical densities than CH_3OH, its

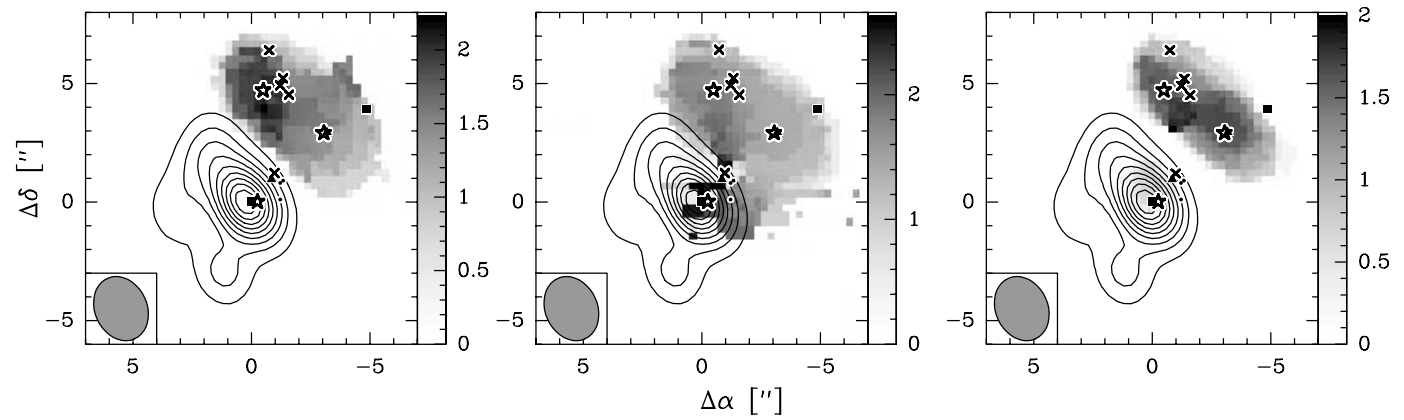

FIG. 8.—Gray scales showing second-moment maps of the NH_3 (1, 1) (*left*) and (2, 2) (*middle*) outermost satellite hyperfine lines and the CH_3OH ($3_{2,1}$–$3_{1,2}$) *E* line (*right*) in NGC 6334I (the wedge in km s^{-1}). The contours in all three panels show the centimeter-continuum data from 10% to 90% of the peak emission of 1197 mJy $beam^{-1}$. The symbols are the same as shown in Fig. 1.

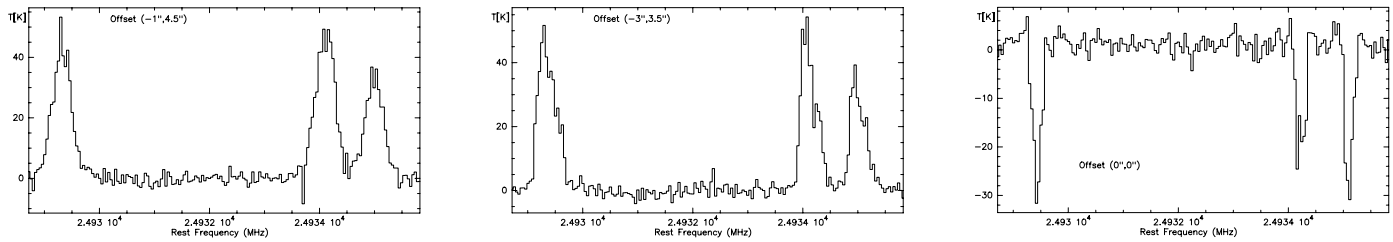

FIG. 9.—CH_3OH spectra taken toward the two emission peaks (*left and middle*) and the UC H II region (*right*) in NGC 6334I. The offsets are given with respect to the phase center listed in Table 1.

line emission shows comparably less contribution from the densest cores, and it is thus more likely to exhibit temperature and kinematic signatures imposed by the adjacent UC H II region.

4.3. *Molecular Absorption toward the UC* H II *Region*

In addition to the molecular line emission, prominent CH_3OH line absorption features are observed in all three lines toward the UC H II region in NGC 6334I (Fig. 9). Examining the NH_3 data, we find no absorption in the satellite hyperfine lines but weak NH_3 absorption features in the two main lines. The *p-v* cuts of one of the CH_3OH and the two NH_3 (1, 1) and (2, 2) main lines through the UC H II region at Δdecl. $= 0$ reveal that the absorption features are blueshifted with regard to the (weak) emission features toward the UC H II region (Fig. 10). This signature is more pronounced in the CH_3OH and NH_3 (1, 1) line, whereas it is not obviously discernible in the NH_3 (2, 2) line. Nevertheless, these data indicate expanding molecular gas around the UC H II region.

5. DISCUSSION

The differences between the two massive star-forming regions NGC 6334I and NGC 6334I(N) in their molecular NH_3 and CH_3OH emission are rather astonishing: compact thermal emission is observed in both species toward the UC H II region/hot core NGC 6334I, whereas extended NH_3 and masing CH_3OH emission is found toward NGC 6334I(N). It is not entirely obvious what is causing these differences because both sources harbor compact millimeter-continuum sources, as well as jetlike SiO outflows (T. R. Hunter et al. 2005, in preparation). Since the southern source NGC 6334I has a UC H II region, it is likely that evolutionary processes are at least partly responsible for the different molecular signatures. However, with the data obtained during the present investigation we still cannot accurately determine temperature and density in both regions, and one expects that the molecular emission is sensitive to these parameters. Therefore, it is an important next step to get thorough estimates of the characteristic temperatures and densities of both regions to get a deeper understanding of the physical processes causing the observational differences.

5.1. *Four Stages of Massive Star Formation within* 1 pc

Figure 11 presents a large-scale overview of the northeastern end of the NGC 6334 region comprising NGC 6334I, NGC 6334E, and NGC 6334I(N). It is interesting that within 1 pc we find four different evolutionary stages of massive star formation: the shell-like H II region NGC 6334E, the champagne flow–like UC H II region NGC 6334I and its adjacent outflow-driving millimeter cores, and farther north the enigmatic source NGC 6334I(N). NGC 6334E lies just outside each of our primary beams; thus, we have no new data about this source.

From an evolutionary point of view, the shell-like H II region NGC 6334E appears to be the most evolved and thus the oldest source within the region (e.g., Rodríguez et al. 1982; Tapia et al. 1996; Carral et al. 2002). The UC H II region NGC 6334I is significantly smaller than NGC 6334E and thus is apparently in an earlier evolutionary stage (e.g., Persi & Ferrari-Toniolo 1982; de Pree et al. 1995). On the basis of the cold dust temperatures, the detection of only a few very red infrared sources, and weak centimeter emission (Gezari 1982; Tapia et al. 1996; Sandell 2000; Carral et al. 2002), NGC 6334I(N) was always considered the youngest region within the large-scale NGC 6334 complex. However, by comparing the millimeter continuum/NH_3 sources in NGC 6334I with those in NGC 6334I(N), it is not entirely obvious which of these two regions is evolutionary younger. Both complexes have compact millimeter–dust continuum sources and drive collimated outflows. In contrast to these similarities, the differences in the compact versus extended NH_3 emission and thermal versus maser CH_3OH emission at 24.9 GHz are striking. Furthermore, the differences in the estimated dust temperatures are large, with 100 K for NGC 6334I and only 30 K for NGC 6334I(N) (Sandell 2000). Contrary to this, even if we constrain only the lower limits for the gas temperatures on the

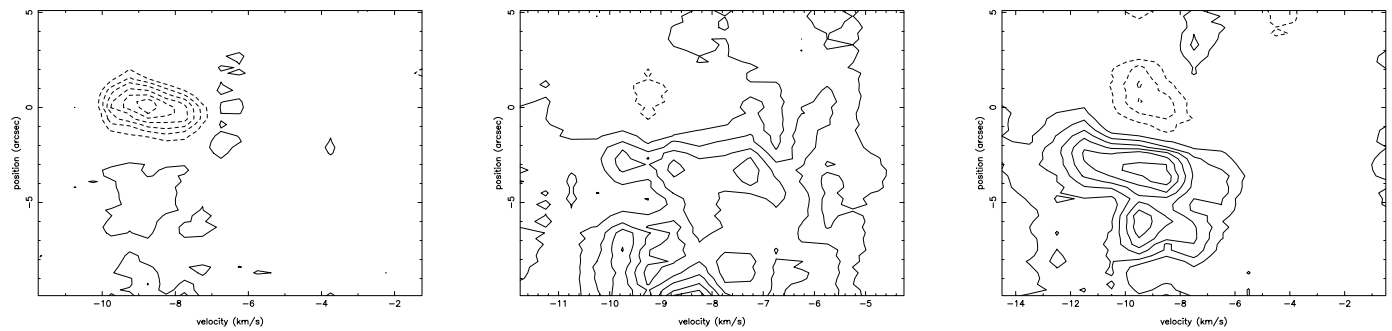

FIG. 10.—Plot of *p-v* cuts in the direction of right ascension at Δdecl. $= 0''$ for the CH_3OH ($3_{2,1}$–$3_{1,2}$) *E* line (*left*) and the two NH_3 (1, 1) (*middle*) and (2, 2) (*right*) main components in NGC 6334I. Positive emission is shown by solid contours, and negative emission is shown by dashed contours. The contour levels are in ± 10, ± 10, and ± 9.5 mJy beam^{-1} steps for the left, middle, and right panels, respectively.

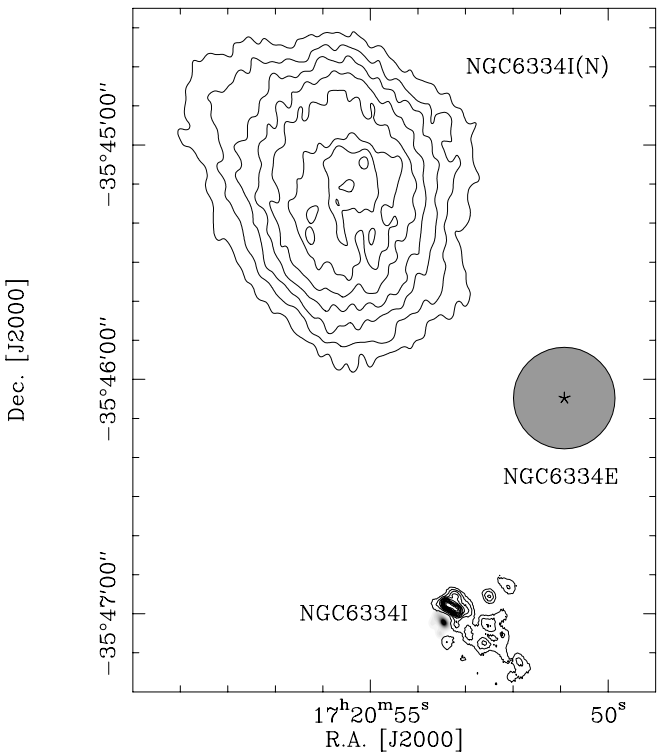

FIG. 11.—Large-scale overview of the northeastern end of the NGC 6334 complex. The gray scale shows the centimeter-continuum emission of NGC 6334I, and the contours present the integrated NH_3 (1, 1) emission of the main hyperfine component. The contour levels are from 10% to 90% of the peak values of each image with the following peak values: centimeter emission, 1197 mJy beam^{-1}; NH_3 (1, 1) in NGC 6334I, 175 mJy beam^{-1}; and NH_3 (1, 1) in NGC 6334I(N), 386 mJy beam^{-1}. The gray circle and star represent the approximate structure of NGC 6334E (e.g., Carral et al. 2002).

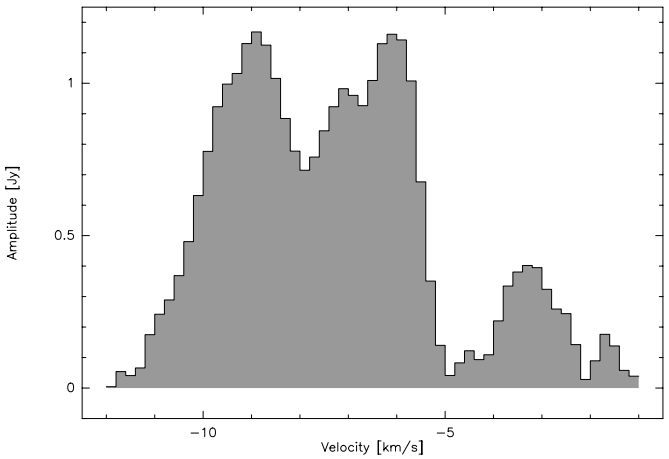

FIG. 12.—NH_3 (1, 1) spectrum of the outer satellite hyperfine component taken in the *u-v* domain on the shortest baseline of 31 m.

basis of our NH_3 observations, we derive kinetic gas temperatures $\geq$100 K for both regions. Even if we consider the different beam sizes of the Submillimeter Common-User Bolometric Array (SCUBA) observations of the dust emission (between 8″.5 and 18″.5, depending on the frequency) and our NH_3 gas observations, the dust and gas temperatures in NGC 6334I appear to be consistent with each other, whereas this is not the case for NGC 6334I(N). There the gas and dust temperatures appear to have decoupled. In addition, Sandell (2000) estimated the bolometric luminosities of both sources to differ by about 2 orders of magnitude, with 2.6×10^5 and 1.9×10^3 $L_\odot$ for NGC 6334I and NGC 6334I(N), respectively. This difference could imply either that NGC 6334I(N) may not form a cluster as massive as NGC 6334I or that NGC 6334I(N) may be less evolved and younger than NGC 6334I and thus may still build up its final larger luminosity. With the observations so far, we cannot clearly judge which of these two regions is in an earlier evolutionary stage. With the UC H II region and the infrared cluster present, the whole region NGC 6334I is older than the region NGC 6334I(N), but it is less clear whether the same conclusion holds for the millimeter/NH_3 cores within NGC 6334I. However, it is worth mentioning that the nondetection of compact NH_3 emission toward the millimeter sources in NGC 6334I(N) is a rarely observed phenomenon and may indicate a short-lived period during the evolution of massive star-forming regions.

5.2. *Turbulence versus Organized Motion*

Figure 12 shows a spectrum of the outermost satellite hyperfine component of the NH_3 (1, 1) line in the *u-v* domain on the shortest baseline of 31 m. Several velocity components are present: one centered at approximately -9 km s^{-1}, one at approximately -6 km s^{-1}, one at approximately -3 km s^{-1}, and one at approximately -1.5 km s^{-1}. Analyzing the spatial distribution of the different velocity components (Fig. 13), we find that only the -9 km s^{-1} component is clearly associated with the southwestern NH_3 emission peak, whereas all other features are associated with the northeastern peak (which is also the peak of stronger millimeter-continuum emission).

Contrary to the complex profile in the *u-v* domain (Fig. 12), the hyperfine components of the spectra taken individually toward each peak position resemble single-peaked Gaussians (Figs. 4 and 6). We performed Gaussian line fits to the outermost satellite hyperfine components of the NH_3 (1, 1) line toward the two NH_3 peak positions in NGC 6334I and the millimeter-peak position in NGC 6334I(N), and the derived line widths Δv vary between 4.1 and 5.1 km s^{-1} (see Table 3).

What is causing these broad line widths—turbulent motion due to, e.g., molecular outflows, or organized motion due to, e.g., infall, envelope rotation, disks, or multiple components? Sridharan et al. (2002) have shown that the NH_3 line width observed with single-dish telescopes toward high-mass protostellar objects (HMPOs) is significantly lower than that toward typical UC H II regions and hot cores ($\Delta v_{\rm HMPO} \sim 2.1$ km s^{-1} vs. $\Delta v_{\rm hc} \sim 3.1$ km s^{-1}, where the subscript "hc" indicates "hot core"). Since we find gas temperatures on the order of 100 K, NGC 6334I and NGC 6334I(N) are considered part of the hot core group. Therefore, most likely the large line widths are an evolutionary signature of the hot core stage and not a remnant from the original molecular core. The thermal line width at 100 K is only 0.31 km s^{-1}, and thus, nonthermal motion has to account for nearly all the observed line width. To estimate the corresponding energy within the core, we calculated $E = (1/2)m\Delta v_{\rm nt}^2$, where m is the core mass derived from the millimeter-continuum emission (T. R. Hunter et al. 2005, in preparation) and $\Delta v_{\rm nt} = (\Delta v^2 - \Delta v_{\rm thml}^2)^{1/2}$ is the nonthermal line width component. The derived energy values corresponding to internal motion are on the order of 10^{46} ergs (see Table 3).

Interestingly, the typical energy supply of massive molecular outflows is on the same order (e.g., Beuther et al. 2002). The spatial scales for the molecular outflows are usually on the order of 1 pc, whereas the NH_3 line widths observed toward NGC 6334I are confined to a few thousand AU; thus, the estimated energies are not directly comparable. However, the uncertainties

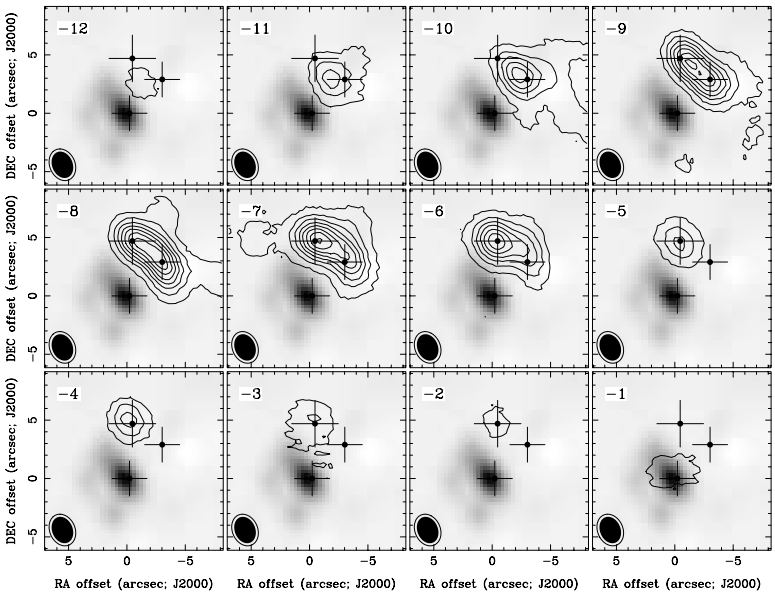

FIG. 13.—Contours present a channel map with 1 km s^{-1} resolution of the NH_3 (1, 1) outer satellite hyperfine component shown in Fig. 12 (contour levels 20, 160, and 20 mJy beam^{-1}). The central velocities are shown at the top left of each panel, and the symbols are the same as in Fig. 1. The gray scale always shows the centimeter-continuum emission.

in deriving outflow energies are usually high, up to an order of magnitude (e.g., Cabrit & Bertout 1990), and it might be possible that comparable amounts of energy could be supplied from the outflow on spatial scales as small as the NH_3 cores. Therefore, turbulence caused by molecular outflows may contribute to the observed line width in NGC 6334I. Contrary to this, Zhang et al. (1998, 2002) find broad NH_3 line widths on the order of 5 km s^{-1} toward two young massive star-forming regions, whereas the NH_3 emission in the surrounding cores has a narrower line width, on the order of 2 km s^{-1}. These observations are interpreted as indirect evidence for rotating disks within these massive star-forming regions. Since we are unable to derive any systematic velocity gradient within the separate cores of NGC 6334I, we cannot attribute our observations to a disk scenario. However, it is likely that the observed line widths are caused at least to some degree by organized motion within the inner few thousand AU caused by either infall, envelope rotation, disks, multiple components, or an interplay of various of these components. Only higher angular resolution observations can disentangle all these contributions.

5.3. *Shocks in NGC 6334I(N)*

In contrast to that in NGC 6334I, the situation appears to be different in NGC 6334I(N) because the NH_3 emission is not confined to the millimeter-peak position, and we observe broad line widths over a large spatial area. Since there are at least two molecular outflows in the region, the broad line width could well be caused by shock interactions of the outflow with the surrounding molecular core.

Additional evidence for outflow-shock interactions is the detection and the spatial spread of the Class I 25 and 44 GHz CH_3OH maser emission, which is believed to be caused by the interactions of outflows from massive star-forming regions with the surrounding cloud cores (e.g., Menten 1991; Sobolev 1993). Class I CH_3OH maser observations at 95 GHz in DR 21 revealed that they are located at the interface of the molecular outflow and the surrounding ambient gas (Plambeck & Menten 1990). Similar results were found for Class I CH_3OH maser emission near 25 GHz in the Orion KL region, where Johnston et al. (1992) suggest that the Class I maser emission is formed behind shock fronts between the outflows and the dense cloud gas.

In the case of NGC 6334I(N), the northeastern 25 GHz maser feature (the −3 km s^{-1} component) is obviously spatially associated with the jetlike SiO (5–4) outflow (T. R. Hunter et al. 2005, in preparation; e.g., Fig. 2) and thus fits well into the shock excitement picture. The southern 25 GHz maser (the −5 km s^{-1} component) is less clearly associated with one of the two outflow axes. However, the northwest-southeastern outflow of Megeath & Tieftrunk (1999) is significantly less collimated than the newly detected SiO jet of T. R. Hunter et al. (2005, in preparation), and therefore, it is plausible that the Class I maser features near the southern −5 km s^{-1} maser peak (i.e., 25 and 44 GHz masers) are associated with the interface of the broader outflow cone and the ambient cloud. When we compare the overall spatial distribution of the 25 and 44 GHz Class I CH_3OH maser emission with the present outflow morphologies (see Fig. 2), all maser features appear to be associated with the outflows and are likely caused by the shock interactions of the outflows and the ambient gas.

The Class I CH_3OH masers in NGC 6334I(N) thus show the same behavior as masers of this kind in many other regions: First, individual narrow-line maser components are spread over areas of several tenths of a pc, offset from any possible exciting source. Additional evidence places them in the interaction zones of outflows and dense ambient gas. Second, apart from perhaps Orion KL, masers in the 44 GHz transition are always

TABLE 3
NH_3 (1, 1) SATELLITE HYPERFINE COMPONENTS

Source	Offset (arcsec)	Δv (km s^{-1})	E (ergs)
NGC 6334I	−1.0, 4.5	5.1	1.2×10^{46}
NGC 6334I	−3.0, 3.5	4.1	4.5×10^{45}
NGC 6334I(N)	6.5, 5.0	4.5	4.8×10^{46}

NOTE.—The line widths are derived from Gaussian fits to the outermost NH_3 (1, 1) hyperfine component at most negative velocities (see Figs. 4 and 6).

stronger than those in any of the 25 GHz lines and are frequently the strongest of all Class I CH_3OH masers. This can be understood from the (collisional) pumping mechanism of Class I methanol masers, which produces efficient masing in the 25 GHz lines over just the range of physical parameters one may expect in the scenario described above (S. Leurini 2005, in preparation). This means that possible 25 GHz emission from many of the spots where 44 GHz emission arises may be too weak to be detectable.

6. SUMMARY

The NH_3 (1, 1) and (2, 2) and CH_3OH observations of the two massive twin cores NGC 6334I and NGC 6334I(N) reveal significantly different emission signatures between the two regions. While NGC 6334I shows strong, compact thermal emission in the observed NH_3 and CH_3OH lines adjacent to the UC H II region and coincident with millimeter-continuum peaks observed by T. R. Hunter et al. (2005, in preparation), there is no compact thermal line emission toward NGC 6334I(N). Here we find that the NH_3 emission is distributed over a broad area of approximately $1'$. No thermal CH_3OH emission is found toward NGC 6334I(N), but we do detect two Class I CH_3OH maser peaks with peak brightness temperatures of $\sim$7000 K. The two maser peaks may be spatially associated with 44 GHz Class I CH_3OH maser emission and are likely produced in the interfaces between the molecular outflows and the ambient gas.

NH_3 peak brightness temperatures >70 K toward the millimeter-peak positions in NGC 6334I and NGC 6334I(N) indicate kinetic temperatures on the same order. However, the NH_3 (1, 1) and (2, 2) lines are only suitable as a good thermometer below 50 K, and thus, we cannot derive more than a lower limit for the temperatures in these regions. Directly at the western edge of the UC H II region we find a hot spot for which the line ratios between the NH_3 (2, 2) and (1, 1) outermost satellite hyperfine components are surprisingly high, around 4, indicating even higher temperatures. Since this position is not associated with any millimeter-continuum peak, the heating is likely caused by the UC H II region. NH_3 emission is also detected toward the outflow in NGC 6334I, and we can estimate a rotational temperature of approximately 19 K there.

Toward the UC H II region in NGC 6334I we observe CH_3OH and NH_3 absorption. The absorption features are blueshifted with regard to the emission features nearby. This signature is consistent with expanding molecular gas around the UC H II region. We do not find additional strong kinematic effects imposed from the UC H II region on the adjacent molecular cores.

We would like to thank Tyler Bourke and Paul Ho for helpful discussions on ATCA and NH_3 during the analysis and interpretation of the data. We are also grateful to an anonymous referee, who commented carefully and in detail on the draft and helped improve it. H. B. acknowledges financial support from the Emmy Noether Program of the Deutsche Forschungsgemeinschaft (grant BE2578/1), and S. T. is grateful to the Alexander von Humboldt Foundation for a Feodor Lynen research fellowship.

REFERENCES

Bachiller, R., & Cernicharo, J. 1990, A&A, 239, 276
Beuther, H., Schilke, P., Sridharan, T. K., Menten, K. M., Walmsley, C. M., & Wyrowski, F. 2002, A&A, 383, 892
Brooks, K. J., & Whiteoak, J. B. 2001, MNRAS, 320, 465
Cabrit, S., & Bertout, C. 1990, ApJ, 348, 530
Carral, P., Kurtz, S. E., Rodríguez, L. F., de Pree, C., & Hofner, P. 1997, ApJ, 486, L103
Carral, P., Kurtz, S. E., Rodríguez, L. F., Menten, K., Cantó, J., & Arceo, R. 2002, AJ, 123, 2574
Danby, G., Flower, D. R., Valiron, P., Schilke, P., & Walmsley, C. M. 1988, MNRAS, 235, 229
Davis, C. J., & Eisloeffel, J. 1995, A&A, 300, 851
De Buizer, J. M., Radomski, J. T., Piña, R. K., & Telesco, C. M. 2002, ApJ, 580, 305
de Pree, C. G., Rodríguez, L. F., Dickel, H. R., & Goss, W. M. 1995, ApJ, 447, 220
Ellingsen, S. P., von Bibra, M. L., McCulloch, P. M., Norris, R. P., Deshpande, A. A., & Phillips, C. J. 1996, MNRAS, 280, 378
Forster, J. R., & Caswell, J. L. 1989, A&A, 213, 339
Gaume, R. A., & Mutel, R. L. 1987, ApJS, 65, 193
Gezari, D. Y. 1982, ApJ, 259, L29
Jackson, J. M., Ho, P. T. P., & Haschick, A. D. 1988, ApJ, 333, L73
Johnston, K. J., Gaume, R., Stolovy, S., Wilson, T. L., Walmsley, C. M., & Menten, P. 1992, ApJ, 385, 232
Kogan, L., & Slysh, V. 1998, ApJ, 497, 800
Kraemer, K. E., Deutsch, L. K., Jackson, J. M., Hora, J. L., Fazio, G. G., Hoffmann, W. F., & Dayal, A. 1999, ApJ, 516, 817
Kraemer, K. E., & Jackson, J. M. 1995, ApJ, 439, L9
———. 1999, ApJS, 124, 439
Kuiper, T. B. H., Peters, W. L., Forster, J. R., Gardner, F. F., & Whiteoak, J. B. 1995, ApJ, 446, 692
Loughran, L., McBreen, B., Fazio, G. G., Rengarajan, T. N., Maxson, C. W., Serio, S., Sciortino, S., & Ray, T. P. 1986, ApJ, 303, 629
McBreen, B., Fazio, G. G., Stier, M., & Wright, E. L. 1979, ApJ, 232, L183
McCutcheon, W. H., Sandell, G., Matthews, H. E., Kuiper, T. B. H., Sutton, E. W. C., Danchi, W. C., & Satō, T. 2000, MNRAS, 316, 152
Megeath, S. T., & Tieftrunk, A. R. 1999, ApJ, 526, L113
Menten, K. 1991, in ASP Conf. Ser. 16, Atoms, Ions, and Molecules: New Results in Spectral Line Astrophysics, ed. A. D. Haschick & P. T. P. Ho (San Francisco: ASP), 119
Moran, J. M., & Rodríguez, L. F. 1980, ApJ, 236, L159
Neckel, T. 1978, A&A, 69, 51
Persi, P., & Ferrari-Toniolo, M. 1982, A&A, 112, 292
Persi, P., Roth, M., Tapia, M., Marenzi, A. R., Felli, M., Testi, L., & Ferrari-Toniolo, M. 1996, A&A, 307, 591
Plambeck, R. L., & Menten, K. M. 1990, ApJ, 364, 555
Rodríguez, L. F., Cantó, J., & Moran, J. M. 1982, ApJ, 255, 103
Sandell, G. 2000, A&A, 358, 242
Sobolev, A. M. 1993, Astron. Lett., 19, 293
Sollins, P. K., & Megeath, S. T. 2004, AJ, 128, 2374
Sridharan, T. K., Beuther, H., Schilke, P., Menten, K. M., & Wyrowski, F. 2002, ApJ, 566, 931
Straw, S. M., & Hyland, A. R. 1989, ApJ, 340, 318
Tapia, M., Persi, P., & Roth, M. 1996, A&A, 316, 102
Thorwirth, S., Winnewisser, G., Megeath, S. T., & Tieftrunk, A. R. 2003, in ASP Conf. Ser. 287, Galactic Star Formation Across the Stellar Mass Spectrum, ed. J. M. De Buizer & N. S. van der Bliek (San Francisco: ASP), 257
Ungerechts, H., Winnewisser, G., & Walmsley, C. M. 1986, A&A, 157, 207
Walmsley, C. M., & Ungerechts, H. 1983, A&A, 122, 164
Zhang, Q., Hunter, T. R., & Sridharan, T. K. 1998, ApJ, 505, L151
Zhang, Q., Hunter, T. R., Sridharan, T. K., & Ho, P. T. P. 2002, ApJ, 566, 982